Eur. Phys. J. A **17**, 19–24 (2003)
DOI 10.1140/epja/i2002-10136-3

THE EUROPEAN PHYSICAL JOURNAL A

Neutron halos in hypernuclei

H.F. Lü[1], J. Meng[1,2,3,a], S.Q. Zhang[1], and S.-G. Zhou[1,2,3]

[1] School of Physics, Peking University, Beijing 100871, PRC
[2] Institute of Theoretical Physics, Chinese Academy of Science, Beijing 100080, PRC
[3] Center of Theoretical Nuclear Physics, National Laboratory of Heavy Ion Accelerator, Lanzhou 730000, PRC

Received: 21 October 2002 / Revised version: 11 January 2003 /
Published online: 8 April 2003 –
Communicated by G. Orlandini

Abstract. Properties of single-Λ and double-Λ hypernuclei for even-N Ca isotopes ranging from the proton dripline to the neutron dripline are studied using the relativistic continuum Hartree-Bogoliubov theory with a zero-range pairing interaction. Compared with ordinary nuclei, the addition of one or two Λ-hyperons lowers the Fermi level. The predicted neutron dripline nuclei are, respectively, ${}^{75}_{\Lambda}$Ca and ${}^{76}_{2\Lambda}$Ca, as the additional attractive force provided by the Λ-N interaction shifts nuclei from outside to inside the dripline. Therefore, the last bound hypernuclei have two more neutrons than the corresponding ordinary nuclei. Based on the analysis of two-neutron separation energies, neutron single-particle energy levels, the contribution of continuum and nucleon density distribution, giant halo phenomena due to the pairing correlation, and the contribution from the continuum are suggested to exist in Ca hypernuclei similar to those that appear in ordinary Ca isotopes.

PACS. 21.10.Gv Mass and neutron distributions – 21.60.-n Nuclear-structure models and methods – 21.60.Jz Hartree-Fock and random-phase approximations – 21.80.+a Hypernuclei

With the rapid development of radioactive ion beam (RIB) factories, nuclear physics has extended its interests to the limits of nuclear existence and to understand the basic physics of the nuclear landscape. New forms and dynamics of nuclei such as neutron skins and halos are explored. More and more exotic nuclei have been investigated since the first case of halo phenomenon in the exotic nucleus ^{11}Li was discovered [1].

Neutron halos can be interpreted as the scattering of Cooper pairs into the continuum, which contains low-lying resonances of small angular momentum, based on the relativistic continuum Hartree-Bogoliubov (RCHB) theory [2]. After successfully describing ^{11}Li [3], giant halos in exotic Zr [4] and Ca [5] nuclei are predicted using the RCHB theory. Although these have not been observed so far, it will be very exciting and challenging for both theorists and experimentalists to explore new exotic nuclear regions, that the present and the planned facilities can reach.

After the first hypernuclear event found in the 1950s [6], much experimental and theoretical effort has been devoted to the investigation of this area of nuclear physics, and a number of comprehensive reviews can be found in refs. [7–13], and references therein. With the additional degree of freedom of strangeness, hypernuclei can provide more information than ordinary nuclei; they add another dimension to weak, electromagnetic or hadronic probes of nuclear dynamics, and can penetrate dense nuclear matter inaccessible to other hadronic probes for the strangeness carried by hyperons. In astrophysics, hyperons also play a significant role in the formation and thermal structure evolution of neutron stars [14].

Using a variety of hypernuclear production reactions and coincidence measurement techniques, data on the single-Λ [15–17] and double-Λ hypernuclei [18–22] have been accumulated. Non-relativistic few-body methods and Skyrme-Hartree-Fock theory have been successfully used to describe single-Λ and double-Λ hypernuclei, see refs. [23,24], and references therein. Relativistic Mean-Field theory (RMF) is one of the most successful approaches for ordinary nuclei [25–27]. It has been applied to describe single and multi-Lambda systems, including the single-particle spectra of Λ-hypernuclei and the spin-orbit interaction, and extended beyond the Lambda to other strange baryons using $SU(3)$ [28–38]. With the strangeness and double charge exchange reaction (K^-, π^+) as a source, prospects for the production of Λ-hypernuclei with a large neutron excess and a neutron halo have been discussed [39]. The single-Λ exotic hypernuclei have been studied in ref. [38]. Here in this paper, motivated by the experimental knowledge of Λ-N interactions and the theoretical understanding on giant

[a] e-mail: mengj@pku.edu.cn

halos [4,5], we present results of a study of the single-Λ and double-Λ hypernuclei of the even-N calcium isotopes, restricted to the spherical case, ranging from the proton dripline to the neutron dripline, with the RCHB theory. Particular attention will be paid to the stability of giant halos in hypernuclei.

In the RMF theory, one describes the nucleons in a nucleus as Dirac spinors (ψ, m) moving in the fields of mesons: isoscalar-scalar meson (σ, m_σ, g_σ), isoscalar-vector meson (ω, m_ω, g_ω), isovector-vector meson ($\vec{\rho}$, m_ρ, g_ρ) and the photon (A). For Λ-hypernuclei, the additional contributions from the Λ particles are included by introducing three new coupling parameters g_σ^Λ, g_ω^Λ and f_ω^Λ, while Λ-hyperons are treated as Dirac spinors ψ_Λ with mass m_Λ. The field tensor for the ω-meson is given as $\Omega_{\mu\nu} = \partial_\mu\omega_\nu - \partial_\nu\omega_\mu$ and by similar expressions for the ρ-meson and the photon. The Lagrangian density including the non-linear self-coupling of the σ field (coupling constants g_2 and g_3) is constructed as

$$\begin{aligned}\mathcal{L} = &\bar{\psi}\left(\not{p} - g_\omega\not{\omega} - g_\rho\not{\vec{\rho}}\vec{\tau} - \frac{1}{2}e(1-\tau_3)\not{A} - g_\sigma\sigma - m\right)\psi \\ &+\bar{\psi}_\Lambda\left(\not{p} - g_\omega^\Lambda\not{\omega} + \frac{f_\omega^\Lambda}{2m_\Lambda}\sigma^{\mu\nu}(\partial_\nu\omega_\mu) - g_\sigma^\Lambda\sigma - m_\Lambda\right)\psi_\Lambda \\ &+\frac{1}{2}\partial_\mu\sigma\partial^\mu\sigma - \frac{1}{2}m_\sigma^2\sigma^2 - \frac{1}{3}g_2\sigma^3 - \frac{1}{4}g_3\sigma^4 \\ &-\frac{1}{4}\Omega_{\mu\nu}\Omega^{\mu\nu} + \frac{1}{2}m_\omega^2\omega_\mu\omega^\mu \\ &-\frac{1}{4}\vec{R}_{\mu\nu}\vec{R}^{\mu\nu} + \frac{1}{2}m_\rho^2\vec{\rho}_\mu\vec{\rho}^\mu - \frac{1}{4}F_{\mu\nu}F^{\mu\nu}\,. \end{aligned} \quad (1)$$

In ref. [36], in order to get more attraction in multi-hyperon hypernuclei, an additional scalar meson σ^* and a vector meson ϕ, which couple only to hyperons, are introduced:

$$\begin{aligned}\mathcal{L}'_{\Lambda\Lambda} = &\frac{1}{4}S_{\mu\nu}S^{\mu\nu} + \frac{1}{2}m_\phi^2\phi_\mu\phi^\mu - g_\phi^\Lambda\overline{\psi}_\Lambda\gamma_\mu\psi_\Lambda\phi^\mu \\ &+\frac{1}{2}(\partial_\nu\sigma^*\partial^\nu\sigma^* - m_{\sigma^*}^2\sigma^{*2}) - g_{\sigma^*}^\Lambda\overline{\psi}_\Lambda\psi_\Lambda\sigma^*, \end{aligned} \quad (2)$$

where $S_{\mu\nu} = \partial_\mu\phi_\nu - \partial_\nu\phi_\mu$ and the coupling constants $g_{\sigma^*}^\Lambda$ and g_ϕ^Λ satisfy $\dfrac{g_\phi^\Lambda}{g_\omega} = -\dfrac{\sqrt{2}}{3}$ and $\dfrac{g_{\sigma^*}^\Lambda}{g_\sigma} = 0.69$.

From the above Lagrangian one can derive the relativistic Hartree-Bogoliubov (RHB) equations; for details see ref. [40]. In the pairing channel a density-dependent two-body force of zero range

$$V(r_1, r_2) = V_0\delta(r_1 - r_2)\frac{1}{4}[1 - \sigma_1\sigma_2]\left(1 - \frac{\rho(r)}{\rho_0}\right) \quad (3)$$

has been used instead of the one-meson exchange interaction, just as was done in refs. [2,3]. The RHB equations for nucleons and the Dirac equations for Λ-hyperons, restricted to spherical symmetry, were solved self-consistently in coordinate space. The detailed formalism and numerical techniques can be found in ref. [2], and references therein.

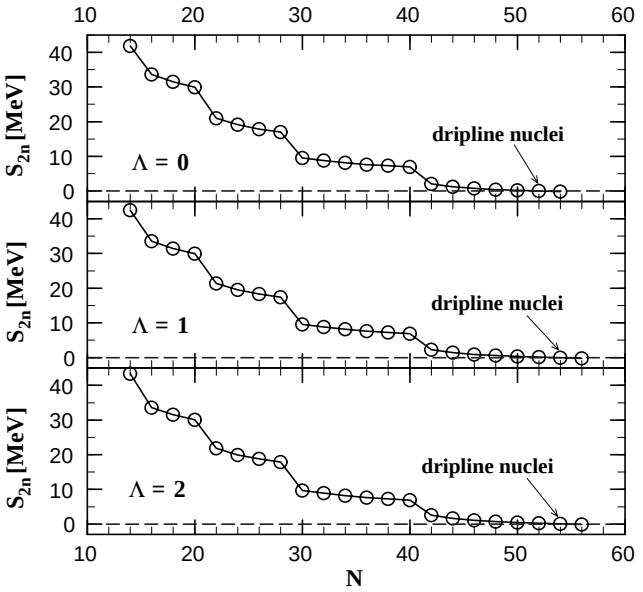

Fig. 1. The two-neutron separation energies S_{2n} in even-N Ca isotopes *versus* the neutron number N. The upper panel is for ordinary nuclei, the middle one for single-Λ hypernuclei, and the lower one for double-Λ hypernuclei.

In the present calculations, we follow the procedures in refs. [2,41] and solve the RCHB equations in a box of size $R = 20$ fm and a step size of 0.1 fm. For nucleons, the parameter set NL-SH [42] was used; it describes properties of nuclear matter as well as of the stable and the exotic nuclei reasonably well. In addition, for lambdas with mass $m_\Lambda = 1115.6$ MeV, the scalar coupling constant $g_\sigma^\Lambda = 0.619g_\sigma$ was chosen to reproduce the binding energy of a Λ in the $1s$ state of ${}^{40}_{\Lambda}$Ca ($B_{1s}^\Lambda = -18.7$ MeV) [16], while the vector coupling constant $g_\omega^\Lambda = 2/3g_\omega^N$ is determined from the naive quark model, where the tensor coupling constant f_ω^Λ is equal to the negative value of g_ω^Λ [43]. The contribution of nucleons in continua was restricted within a cut-off energy $E_{\rm cut} \sim 120$ MeV. For fixed cut-off energy and for fixed box radius R, the strength $V_0 = -650$ MeV fm^{-3} of the zero-range pairing force was determined by adjusting the corresponding pairing energy $-\frac{1}{2}\mathrm{Tr}\Delta\kappa$ to that of a RCHB calculation using the finite-range part of the Gogny force DIS, as in ref. [2]. For ρ_0 in the pairing force, we used the nuclear matter density 0.152 fm^{-3}. The pairing correlation for hyperons was neglected and the spinor wave function was obtained by solving the corresponding Dirac equation. The whole system, including hyperons, nucleons and mesons was solved self-consistently in the usual mean-field approximation. The calculation for the Lagrangian $\mathcal{L}$ will be presented below. The contribution of the terms $\mathcal{L}'_{\Lambda\Lambda}$ with $m_{\sigma^*} = 975$ MeV and $m_\phi = 1020$ MeV has also been done and will be discussed subsequently.

In fig. 1 we show the theoretical two-neutron separation energy S_{2n} for ordinary nuclei, single-Λ hypernuclei and double-Λ hypernuclei of Ca isotopes, labelled by $\Lambda = 0$, $\Lambda = 1$ and $\Lambda = 2$, respectively, from the proton dripline to the neutron dripline. The common property among them is: along the S_{2n} *versus* N curve, three

Table 1. Nuclear Fermi energies (in MeV) for nuclei close to the neutron dripline. N is the neutron number and λ is the Fermi energy.

	λ_n			λ_p		
N	^{A}Ca	${}^{A+1}_{\Lambda}$Ca	${}^{A+2}_{2\Lambda}$Ca	^{A}Ca	${}^{A+1}_{\Lambda}$Ca	${}^{A+2}_{2\Lambda}$Ca
52	−0.067	−0.102	−0.141	−26.165	−26.384	−26.976
54	0.010	−0.022	−0.057	−26.482	−26.710	−27.390
56	0.089	0.062	0.030	−26.302	−26.953	−27.566

strong kinks appear at the magic or submagic numbers $N = 20, 28$, and 40. However, there is no kink at the traditional magic number $N = 50$, which is due to the disappearance of the energy gap between the $1g_{9/2}$ orbit and the usually higher-lying s-d shell. Similarly, there is no kink at $N = 50$ in the chemical potential curve due to the lowering of the $3s_{1/2}$ and $2d_{5/2}$ orbits. It was found that the extra Λ-hyperons do not break the neutron shell structure, as can be seen clearly in fig. 4 below. However, the neutron dripline is pushed outward from $N = 52$ in the ordinary isotope chain to $N = 54$ in the hyper-isotope chain. This is a slight but rewarding step for exploring the limit of the existence of dripline nuclei, and is a manifestation of the giant halo. To make this more quantitative, nuclear Fermi energies for nuclei around the neutron dripline are listed in table 1. The Fermi level is lowered in hypernuclei compared with that in ordinary nuclei; embedding one or two Λ's into the ordinary nuclei can change an unbound nucleus core into a bound one. The neutron Fermi energy at $N = 54$ is reduced from 0.010 MeV in ordinary neutron dripline nuclei to −0.022 MeV in single-Λ hypernuclei and −0.057 MeV in double-Λ hypernuclei, *i.e.*, ${}^{75}_{\Lambda}$Ca and ${}^{76}_{2\Lambda}$Ca are bound neutron-rich hypernuclei.

Another remarkable common property seen in fig. 1 is that the S_{2n} values for exotic Ca isotopes are extremely close to zero in isotopes with neutron number larger than 40. If one regards ^{60}Ca as a core, then the valence neutrons are filled in the weakly bound levels and continuum above the $N = 40$ subshell for these nuclei. As mentioned in ref. [5], the nuclei ${}^{62\text{-}72}$Ca, which are unbound without pairing, become bound with the contribution from $1g_{9/2}$ and $3s_{1/2}$ in the continuum. The small two-neutron separation energies in ordinary nuclei resulting from the giant halo exist also in the Ca hypernuclei, just as in the Zr chain [4]. This can be well understood from the effect of the added Λ's on the single-particle energy levels near the threshold [44].

One of the characteristics of the halo or giant halo is the large space extension of the nuclear density distribution. In fig. 2, the neutron density distributions in both normal and logarithmic scales for single-Λ and double-Λ hypernuclei of Ca isotopes are presented. From the logarithmic scale figures, we can see that the distribution for isotopes with $N > 40$ extend well beyond the lighter ones. For example, the tail of ${}^{72}_{\Lambda}$Ca is 10^4 times larger than that of ${}^{42}_{\Lambda}$Ca at $r = 11$ fm.

To further illustrate the neutron giant halo phenomena in hypernuclei, the calculated root-mean-square radii

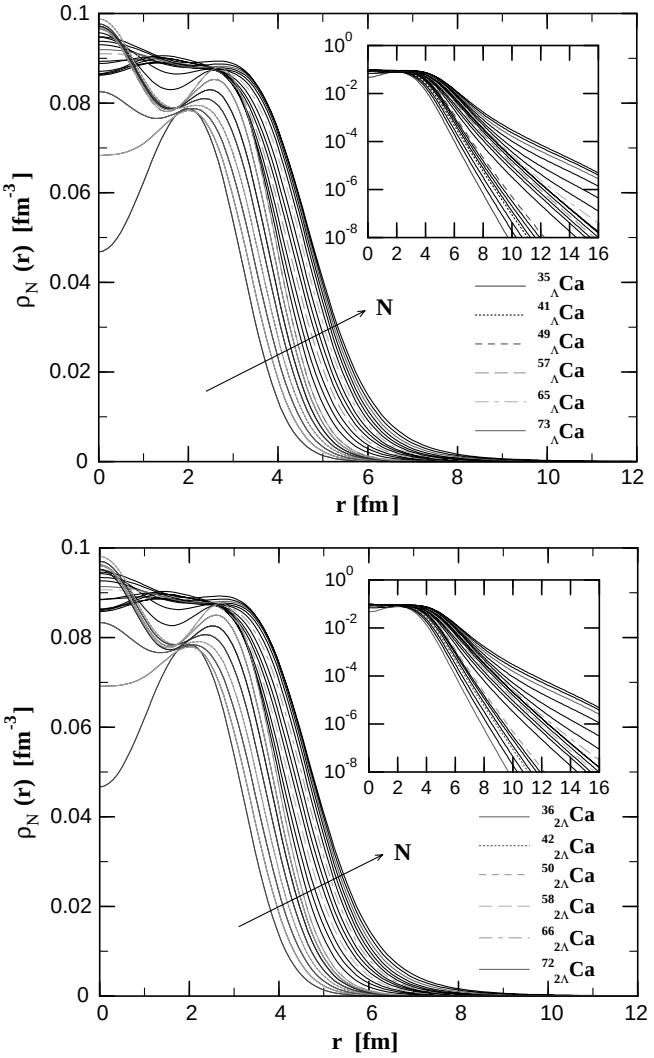

Fig. 2. Neutron density distributions in normal and logarithmic scales for all even Ca isotopes with one or two Λ-hyperons.

of neutron (r_n), lambda (r_Λ), total matter (r_m) as well as charge radii (r_c) from the RCHB calculation for ordinary nuclei, and of single-Λ and double-Λ hypernuclei of even-N Ca isotopes, are plotted as a function of N in fig. 3. Except a slight decrease for r_n and r_m in the exotic region, r_n, r_m and r_c of the ordinary nuclei and the hypernuclei almost overlap with each other. The slight decreases in the exotic region suggest a shrinkage of the nuclear core. This corresponds to the shift of the dripline nuclei and the change from an unbound core nucleus to a bound one. Furthermore, near the neutron dripline, abnormal behavior breaking the $N^{1/3}$ systematic rule appears at $N = 40$ in Ca isotopes with a more rapid than usual increase of r_n with neutron number. It gives further support for the formation of the giant halo. Although the Λ-N interaction cannot stabilize the core $A = 140$ in ${}^{141}_{\Lambda}$Zr [38], it does stabilize the core in ^{74}Ca. Obviously, the giant halo in Ca isotopes, especially in hypernuclei, will be more easily accessed experimentally than that in Zr isotopes.

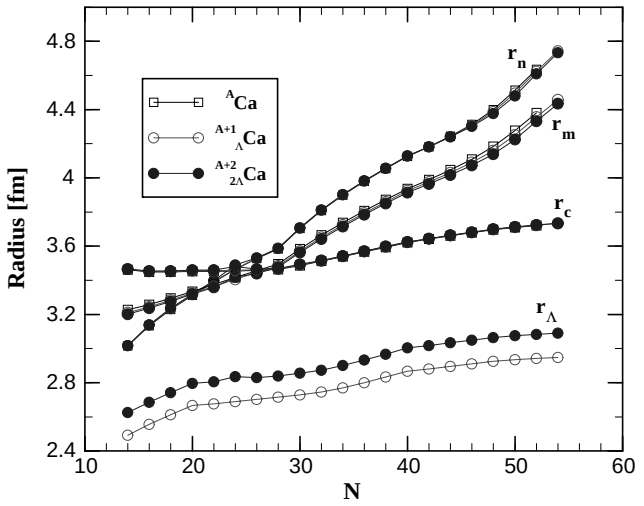

Fig. 3. The root-mean-square radii of neutrons, lambdas, matter, and charge radii from the RCHB calculation for ordinary, single-Λ and double-Λ even-N Ca isotopes as a function of the neutron number N.

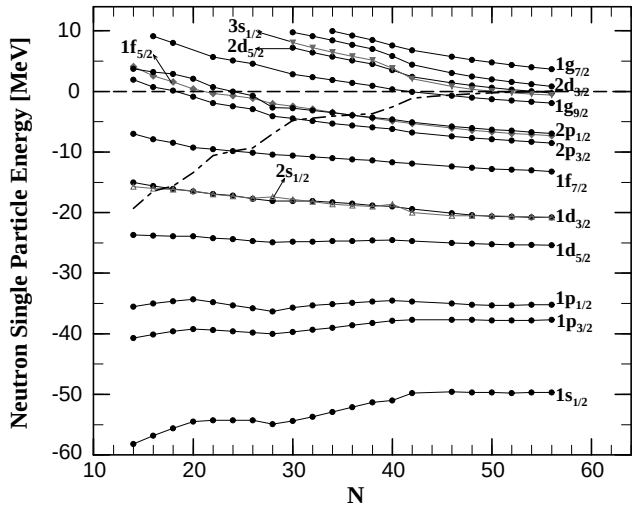

Fig. 4. Neutron single-particle energies in the canonical basis for the double-Λ hypernuclei of even-N Ca isotopes from the neutron number $N = 14$ to $N = 44$.

To understand the above results more clearly, the microscopic structure of the single-particle spectrum in the canonical basis has been given in fig. 4, where the neutron single-particle levels in the canonical basis are shown for the even double-Λ Ca isotopes ranging from the mass number $A = 36$ to $A = 76$. The shell closure ($N = 20, 28$) and subshell closure ($N = 40$) can be clearly seen as large gaps between levels. A dot-dashed line in the figure represents the neutron chemical potential λ_n, which jumps three times at magic or submagic neutron number on its way to the dripline nucleus $^{76}_{2\Lambda}$Ca. As mentioned above, similar kinks appear in the S_{2n} results. These jumps correspond to the shell (or subshell) closure. As the chemical potential λ_n approaches zero, the Ca isotopes with $N > 40$ are all weakly bound, as the pairing correlation will scatter the neutron pairs from bound states to continuum states.

Table 2. The single-particle energies ϵ_i (in MeV) for the last bound state $1g_{9/2}$ and several states in the continuum, together with their corresponding neutron numbers $(2j+1)n_{\rm occ}$, on these state for ^{66}Ca and $^{68}_{\Lambda}$Ca.

	Nuclei	$1g_{9/2}$	$3s_{1/2}$	$2d_{5/2}$	$2d_{3/2}$	$1g_{7/2}$
$(2j+1)n_{\rm occ}$	^{66}Ca	5.14	0.178	0.426	0.108	0.136
	$^{68}_{\Lambda}$Ca	5.32	0.120	0.360	0.084	0.120
ϵ_i	^{66}Ca	−0.48	0.64	1.41	2.85	5.67
	$^{68}_{\Lambda}$Ca	−0.71	0.81	1.40	3.06	5.72

Thus the additional neutrons occupy either weakly bound states or the continuum and they supply very little binding energy. So, levels near the Fermi surface in the order $1g_{9/2}$, $3s_{1/2}$, $2d_{5/2}$, $2d_{3/2}$, etc., will assume an important role, as discussed below.

Taking ^{66}Ca and $^{68}_{\Lambda}$Ca as examples, the neutron single-particle levels in the canonical basis are given in fig. 5. The central potentials are represented by the solid curves. The deepest central potentials for ^{66}Ca and $^{68}_{\Lambda}$Ca are −69.23 MeV and −71.25 MeV, respectively, a 3% change. The length of the line representing each level is proportional to its occupation probability. The root-mean-square radius $r_{nlj} = \sqrt{(\int \rho_{nlj} r^2 {\rm d}\tau)/(\int \rho_{nlj} {\rm d}\tau)}$ for each level is shown in fm in parentheses behind the corresponding label. The neutron Fermi surface is shown by the dashed line, which is −0.607 MeV for $^{68}_{\Lambda}$Ca and −0.435 MeV for ^{66}Ca. The single-particle energies for the last bound state $1g_{9/2}$ and several states in the continuum, together with the corresponding particle numbers on these state for ^{66}Ca and $^{68}_{\Lambda}$Ca, are shown in table 2. By adding two Λ's to ordinary nuclei, the neutron numbers in the continuum decrease slightly, while the neutron single-particle levels rise slightly. Conversely, the binding energy of the last bound state, $1g_{9/2}$, increases, as does the occupation number. This means that neutrons are bound more strongly than in nuclei without Λ. The radius of the $3s_{1/2}$ state, which contributes to the nuclear r.m.s. radius considerably, is reduced from 7.24 fm to 6.96 fm. Correspondingly, the total neutron radius decreases from 4.314 fm to 4.303 fm. Nevertheless, the root-mean-square radius of the $3s_{1/2}$ state in hypernuclei is much larger than the r.m.s. radii of the neighbor states ($\sim$ 5 fm) and the total neutron radius (4.31 fm) due to the zero centrifugal barrier. As a result, the neutron radii for single-Λ and double-Λ hypernuclei of even-N Ca isotopes increase rapidly with neutron number near the dripline, similar to those for ordinary Ca isotopes [5]. Thus, the giant neutron halos also exist in hypernuclei. Of course, the hypernuclear lifetimes may be too short for their neutron density distributions to be measured, but our experimental-physics colleagues may be able to rise to this challenge, just as they did for the halos in excited states for ordinary nuclei [45].

Finally, we examine the contribution of the terms $\mathcal{L}'_{\Lambda\Lambda}$ with $m_{\sigma^*} = 975$ MeV and $m_\phi = 1020$ MeV to see whether the above conclusions still hold. As examples, the total binding energy B, energies of the scalar meson E_{σ^*} and

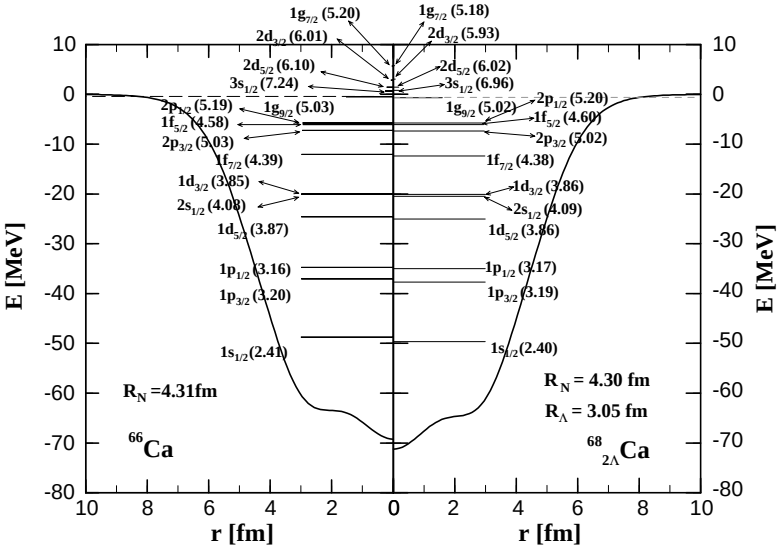

Fig. 5. Neutron single-particle spectra in the canonical basis for ^{66}Ca and $^{68}_{2\Lambda}$Ca. The neutron potential $V(r)+S(r)$ is represented by the solid curve and the Fermi surface is shown as a dashed line. The occupation probabilities for the single-particle levels are proportional to their length. The root-mean-square radius r_{nlj} for each orbit is shown in fm in parentheses behind the corresponding label.

Table 3. Total binding energy B, energies of the scalar meson E_{σ^*} and vector meson E_ϕ, and the Fermi levels (all in MeV) for neutrons, protons and hyperons in $^{72\text{-}78}_{2\Lambda}$Ca with and without $\mathcal{L}'_{\Lambda\Lambda}$.

Lagrangian	Nuclei	B	E_{σ^*}	E_ϕ	λ_n	λ_p	λ_Λ
$\mathcal{L}$	$^{72}_{\Lambda\Lambda}$Ca	511.696			−0.251	−25.852	−19.666
	$^{74}_{\Lambda\Lambda}$Ca	511.919			−0.141	−26.644	−19.760
	$^{76}_{\Lambda\Lambda}$Ca	511.970			−0.057	−27.391	−19.835
	$^{78}_{\Lambda\Lambda}$Ca	511.871			0.030	−27.060	−19.903
$\mathcal{L}+\mathcal{L}'_{\Lambda\Lambda}$	$^{72}_{\Lambda\Lambda}$Ca	512.373	3.173	−2.473	−0.248	−26.316	−20.198
	$^{74}_{\Lambda\Lambda}$Ca	512.590	3.151	−2.456	−0.139	−26.945	−20.288
	$^{76}_{\Lambda\Lambda}$Ca	512.638	3.137	−2.445	−0.056	−27.286	−20.360
	$^{78}_{\Lambda\Lambda}$Ca	512.537	3.126	−2.436	0.032	−26.507	−20.426

vector meson E_ϕ, and the Fermi levels for the neutrons, protons and hyperons in $^{72\text{-}78}_{2\Lambda}$Ca with and without $\mathcal{L}'_{\Lambda\Lambda}$ are listed in table 3. The net contribution from the scalar meson σ^* and vector meson ϕ to the total binding energy B is less than 1 MeV in all cases. The changes of the neutron Fermi levels and the tendency of the two-neutron separation energy are negligible. Therefore, we conclude that these new terms in the Lagrangian do not change the present results.

In summary, the ground-state properties of single-Λ and double-Λ hypernuclei of even-N Ca isotopes from the proton dripline to the neutron dripline have been investigated within the self-consistent relativistic continuum Hartree-Bogoliubov theory. One or two Λ-hyperons embedded into ordinary nuclei do change the bulk properties of the core nucleus, such as the binding energy, the root-mean-square radius, and the central potential, slightly. The weak attractive force resulting from the additional Λ moves the Fermi level slightly. And it is interesting to note that the dripline nucleus for hypernuclei of Ca is at $N = 54$ compared with that for ordinary nuclei at $N = 52$, due to the presence of one or two Λ-hyperons. Based on the two-neutron separation energy S_{2n}, r.m.s. radii, single-particle levels spectra and the contribution of the continuum, giant halo phenomena still exist in hypernuclei with embedded Λ-hyperons in the Ca isotopes. It should be noted that, as in ref. [5], $N = 50$ is no longer a magic number at the neutron dripline. This is due to the halo property of the neutron density within the spherical nuclei, as opposed to the disappearance of the $N = 20$ magic number due to deformation. So far, all the calculations have been done with the assumption of spherical symmetry. Whether these nuclei near the dripline are deformed or not is a very interesting topic. Although the deformed RMF in coordinate space has been reported in ref. [46], its extension to include pairing self-consistently is still in progress; these questions will be addressed in the future.

We would like to express our sincere gratitude to Richard Boyd from Ohio State University for his careful reading of the manuscript. This work was partly supported by the Major State Basic Research Development Program Under Contract

Number G2000077407 and the National Natural Science Foundation of China under Grant Nos. 10025522, 10047001, and 19935030.

References

1. I. Tanihata *et al.*, Phys. Rev. Lett. **55**, 2676 (1985).
2. J. Meng, Nucl. Phys. A **635**, 3 (1998).
3. J. Meng, P. Ring, Phys. Rev. Lett. **77**, 3963 (1996).
4. J. Meng, P. Ring, Phys. Rev. Lett. **80**, 460 (1998).
5. J. Meng, H. Toki, J.Y. Zeng, S.Q. Zhang, S.G. Zhou, Phys. Rev. C **65**, R041302 (2002).
6. M. Danysz, J. Pniewski, Philos. Mag. **44**, 348 (1953).
7. R.E. Chrien, C.B. Dover, Annu. Rev. Nucl. Part. Sci. **39**, 113 (1989).
8. C.B. Dover, D.J. Millener, A. Gal, Phys. Rep. **184**, 1 (1989).
9. H. Bandō, T. Motoba, J. Žofka, Int. Mod. Phys. A **5**, 4021 (1990).
10. B.F. Gibson, E.V. Hungerford, Phys. Rep. **257**, 349 (1995).
11. Y. Akaishi, T. Yamazaki, Prog. Part. Nucl. Phys. **39**, 565 (1997).
12. E. Oset, A. Ramos, Prog. Part. Nucl. Phys. **41**, 191 (1998).
13. W.M. Alberico, G. Garbarino, Phys. Rep. **369**, 1 (2002).
14. M. Prakash, J.U. Lattimer, Nucl. Phys. A **639**, 433c (1998).
15. R.H. Dalitz *et al.*, Proc. R. Soc. London A **426**, 1 (1989).
16. P.H. Pile *et al.*, Phys. Rev. Lett. **66**, 2585 (1991).
17. H. Hotchi *et al.*, Phys. Rev. C **64**, 044302 (2001).
18. M. Danysz *et al.*, Nucl. Phys. **49**, 121 (1963); R.H. Dalitz *et al.*, Proc. R. Soc. London A **426**, 1 (1989).
19. D. Prowse, Phys. Rev. Lett. **17**, 782 (1966).
20. S. Aoki *et al.*, Prog. Theor. Phys. **85**, 1287 (1991).
21. J.K. Ahn *et al.*, Phys. Rev. Lett. **87**, 132504-1(2001).
22. H. Takahashi *et al.*, Phys. Rev. Lett. **87**, 212502-1 (2001).
23. I.N. Filikhin, A. Gal, Phys. Rev. C **65**, 041001 (2002).
24. D.E. Lanskoy, Phys. Rev. C **58**, 3351 (1998).
25. B.D. Serot, J.D. Walecka, Adv. Nucl. Phys. **16**, 1 (1986).
26. P-G Reinhard, Rep. Prog. Phys. **52**, 439 (1989)
27. P. Ring, Prog. Part. Nucl. Phys. **37**, 193 (1996).
28. J. Boguta, S. Bohrmann, Phys. Lett. B **102**, 93 (1981).
29. R. Brockmann, W. Weise, Nucl. Phys.A **355**, 365 (1981).
30. M. Rufa, H. Stöcker, J. Maruhn, P.-G. Reinhard, W. Greiner, J. Phys. G **13**, 143 (1987).
31. J. Mareš, J. Žofka, Z. Phys. A **333**, 209 (1989). Phys. Lett. B **249**, 181 (1990).
32. M. Rufa, J. Schaffner, J. Maruhn, H. Stöcker, W. Greiner, P.-G. Reinhard, Phys. Rev. C **42**, 2469 (1990).
33. M. Chiapparini, A.O. Gattone, B.K. Jennings, Nucl. Phys. A **529**, 589 (1991).
34. J. Schaffner, C. Greiner, H. Stöcker, Phys. Rev. C **46**, 322 (1992).
35. J. Mareš, B.K. Jennings, Phys. Rev. C **49**, 2472 (1994).
36. J. Schaffner, C. Dover, A. Gal, C. Greiner, D. Millener, H. Stöcker. Ann. Phys. (N.Y.) **235**, 35 (1994).
37. Z.Y. Ma, J. Speth, S. Krewald B.Q. Chen, A. Reuber, Nucl. Phys. A **608**, 305 (1996).
38. D. Vretenar, W. Pöschl, G.A. Lalazissis, P. Ring, Phys. Rev. C **57**, R1060 (1998).
39. L. Majling, Nucl. Phys. A **585**, 211c (1995).
40. H. Kucharek, P. Ring, Z. Phys. A **339**, 23 (1991).
41. J. Meng, I. Tanihata, S. Yamaji, Phys. Lett. B **419**, 1 (1998).
42. M.M. Sharma, M.A. Nagarajan, P. Ring, Phys. Lett. B **312**, 377 (1993).
43. J. Cohen, H.J. Weber, Phys. Rev. C **44**, 1181 (1991).
44. J. Meng, I. Tanihata, Nucl. Phys. A **650**, 176 (1999).
45. Z.H. Liu *et al.*, Phys. Rev. C **64**, 034312 (2001).
46. S.G. Zhou, J. Meng, S. Yamaji, S.C. Yang, Chin. Phys. Lett. **17**, 717 (2000).